Earth Planet. Sci. Lett. 647 (2024) 119021

Contents lists available at ScienceDirect

Earth and Planetary Science Letters

journal homepage: www.elsevier.com/locate/epsl

# A distinct type of MORB formed by two-stage melting of a hybrid mantle during Gondwana breakup

Maxim Portnyagin [a,*], Antje Dürkefälden [a], Folkmar Hauff [a], Andrey Gurenko [b], Daniel A. Frick [c], Dieter Garbe-Schönberg [c], Kaj Hoernle [a,c]

[a] GEOMAR Helmholtz Centre for Ocean Research Kiel, Kiel, Germany
[b] Centre de Recherches Pétrographiques et Géochimiques (CRPG), Université de Lorraine, Vandœuvre-lès-Nancy, France
[c] Institute of Geosciences, Kiel University, Kiel, Germany

ARTICLE INFO

Editor: Dr R. Hickey-Vargas

*Keywords:*
Indian Ocean
MORB
Continental breakup
Two-stage melting
Mantle preconditioning

ABSTRACT

The nature of magmatism associated with the breakup of the Gondwana supercontinent remains controversial. Here we report compositions of volcanic glasses from Jurassic (~155 Ma) seafloor adjacent to the Investigator Ridge, providing new insights on magma generation in the embryonic Indian Ocean. These samples have exceptionally primitive compositions with the highest MgO (~10.6 wt%) content found thus far in mid-ocean-ridge basalt (MORB) glasses globally. They also have FeO-rich (~10 wt%) compositions, strongly fractionated HREE patterns (Dy/Yb ~1.24 versus 1.4–1.5 in the prevailing mantle), highly depleted contents of moderately incompatible elements (Zr, MREE) but elevated contents of highly incompatible elements and enriched Sr–Nd–Hf–Pb isotopic characteristics. A long-lived and hot mantle plume may not be required to explain the composition of these basalts associated with more typical but also Fe-rich MORB in the Argo Basin. Instead, we propose that these magmas can originate at normal or only moderately elevated temperatures from less magnesian mantle consisting of undepleted high-Mg# peridotite and residual, previously melted under thick continental lithosphere low-Mg# eclogite, likely MORB-like recycled oceanic crust. Re-melting of such hybrid mantle occurred during continental breakup, possibly due to induced active upwelling at continental edges and involved interaction with trace element and isotopically enriched subcontinental lithosphere. Together with basalts from the Red Sea deeps, the Jurassic rocks from the Indian Ocean represent a distinct type of MORB formed by multi-stage melting of lithologically heterogeneous mantle during continental breakup.

## 1. Introduction

Continental breakup is often associated with volcanism of variable magnitude that leads to either volcanic rifted margins or magma poor margins. The origin of this volcanism is commonly believed to result from extension and decompression melting over a large-scale thermal mantle anomaly usually explained by upwelling of deep mantle in plumes (e.g., Courtillot et al., 1999; Hill et al., 1992; White and McKenzie, 1989). However, along a number of continental margins, initial ocean opening was not related to spatial or temporal progressions of magmatism that can be associated with mantle plumes (hot-spots) (see review Franke, 2013 and references therein). Alternative explanations for locally enhanced volcanism at continental breakup propose thermal insulation and increase of asthenospheric temperature beneath a continent (Grigné and Labrosse, 2001; Coltice et al., 2007; Brandl et al., 2013). Other models of continental breakup emphasize the importance of the rifting history that together with mantle temperature controls the volume of rift-related magmatism (Armitage et al., 2010; Ligi et al., 2011; 2012), whereas other models propose that mantle fertility controls melt production (Korenaga, 2004; Anderson, 2005).

The evolution of the Indian Ocean since the beginning of its formation is very complex and still not fully understood (e.g., Gibbons et al., 2012; Seton et al., 2012). Opening of the Eastern Indian Ocean started with the breakup of East Gondwana and the onset of continental rifting between India, West Australia and West Burma (or Argoland) at around 160 Ma and shortly thereafter Antarctica (Müller et al., 2019; Seton et al., 2012), which later progressed to seafloor spreading. The NW Australian offshore area has long been considered to be a volcanic rifted margin with some volcanism predating continental breakup (White and McKenzie, 1989; Crawford and von Rad, 1994; Rohrman, 2013; 2015,

* Corresponding author.
*E-mail address:* mportnyagin@geomar.de (M. Portnyagin).

https://doi.org/10.1016/j.epsl.2024.119021
Received 29 January 2024; Received in revised form 9 September 2024; Accepted 17 September 2024
Available online 29 September 2024

Magee and Jackson, 2020).

The oldest oceanic crust in the Eastern Indian Ocean with an age of ~154 Ma (magnetic anomaly M26, Gibbons et al., 2012; K/Ar age = 155.3 ± 6.8 Ma (2σ), Ludden, 1992) has been recovered at ODP Leg 123 Site 765 in the Argo Abyssal Plain at the northern tip of the West Australian margin (Fig. 1a). Ludden and Dionne (1992) noted some geochemical similarities between the composition of volcanic rocks from the Argo Abyssal Plain and the Red Sea and proposed that their composition may reflect high degrees of mantle melting associated with an enhanced thermal gradient below recently rifted continental lithosphere. Strongly depleted trace element and isotope compositions of the Argo basalts were, however, considered inconsistent with a mantle plume origin. Crawford and von Rad (1994) reported compositions of ~155 Ma geochemically diverse Fe-rich tholeiitic to alkali basalts dredged from the Rowley Terrace – Scott Plateau margin and from the SW corner of the Exmouth Plateau (Fig. 1a). The authors noted a close similarity in composition of these rocks to those of the southern Red Sea – Gulf of Aden. They questioned a plume-related origin due to 1) the apparent absence of a large igneous province in northern Australia predating the continental breakup and 2) rapid transition from enriched (plume-type) activity to highly trace element and isotopically depleted magmatism along the Argo spreading center. Thus, the origin of compositionally diverse, but relatively small volume volcanism during the Gondwana continental breakup remains largely unconstrained, in part due to strong alteration of these old submarine samples and their rarity.

Another, not yet studied, fragment of the Late Jurassic oceanic crust in the Eastern Indian Ocean was preserved directly west of the southern Investigator Ridge (Fracture Zone) in the Wharton Basin (Fig. 1a). Rock samples from this crustal block, which appears as several ridge- and plateau-like structures rising ~1000 m above the surrounding seafloor and separated from the Investigator ridge and from each other by canyons, were recovered during R/V SONNE cruise SO199 CHRISP (dredge haul DR30; 16°47.04′S, 98°47.50′E, 4586 m.b.s.l.) (Werner et al., 2009; Dürkfälden et al., 2024). $^{40}Ar/^{39}Ar$ dating of volcanic glass from this dredge revealed an age of 155.6 ± 3.4 Ma (2σ) (the age of 153.1 ± 3.3 Ma from Gibbons et al. (2012) has been recalculated here using the decay constants of Steiger and Jäger (1977) and the flux monitor ages of Fleck et al. (2019)). Based on plate tectonic reconstructions, Gibbons et al. (2012) interpreted the Jurassic crust near the Investigator Ridge to have formed at the western extension of the Argo spreading center (Fig. 1b) and that several spreading reorganizations transferred it to its present-day location near the Investigator Ridge on the Australian Plate.

In this paper we report the results of a detailed geochemical study of Jurassic basaltic glasses from the Investigator Ridge, as well as new data on ODP Leg 123 Site 765 basaltic glasses from the Argo Abyssal Plain (Fig. 1a). We show that parental magmas of the oldest Indian Ocean crust originate from lithologically heterogeneous mantle variably depleted during the early stages of continental breakup and then re-melted at the beginning of ocean rifting. The data contribute to refining tectonic models for the Indian Ocean and suggest the existence of a distinct type of MORB magma likely originated from a hybrid mantle source, which may be indicative of the initial stages of ocean spreading.

## 2. Methods

### 2.1. Sample preparation

The glassy margins of the pillow lava samples were carefully crushed in a steel mortar, repeatedly washed with deionized water and dried in an oven at 50 °C. Visibly fresh glass chips were hand-picked under a binocular microscope and then embedded in a mount using a two-component epoxy resin for major and trace element analyses. About 200 mg of visibly fresh glass chips were also hand-picked from the 0.5–1 mm fraction under a binocular microscope for isotope analyses. The glass freshness was confirmed by analytical data on randomly selected chips, which indicated low $H_2O$ content and no selective enrichment in Cs, U, K, Rb, Sb, As, and B, usually associated with low temperature MORB glass alteration (e.g., Jochum and Verma, 1996).

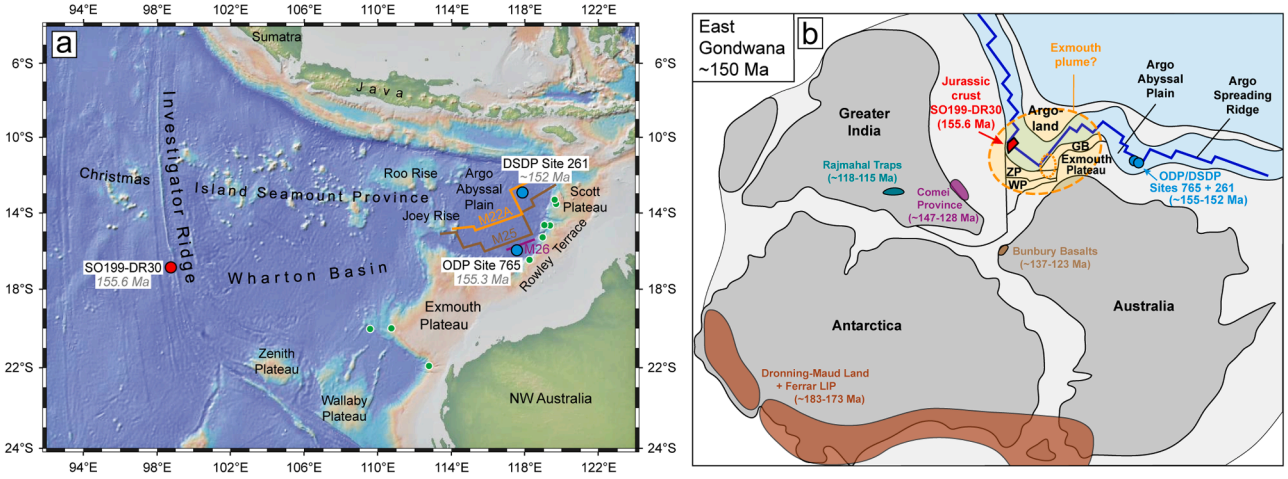


**Fig. 1.** Northeastern Indian Ocean and tectonic reconstruction of East Gondwana during ocean opening.
a) Bathymetric map of the northeastern Indian Ocean showing the location of the DR30 glasses (red circle) sampled during cruise SO199 CHRISP (Ar/Ar age from Gibbons et al., 2012) and belonging to a Jurassic sliver of oceanic crust near the Investigator Ridge. Locations of ODP Leg 123 Site 765 (K/Ar age from Ludden, 1992) and DSDP Leg 27 Site 261 in the Argo Abyssal Plain are also shown (blue circles). Selected magnetic lineations are from Gibbons et al. (2012) with chron ages of 154.2 Ma for M26, 153.2 Ma for M25 and 149.2 Ma for M22A (Ogg, 2020). Small green circles show locations of dredges at the NW Australian margin, which recovered magmatic rocks, from Crawford and von Rad (1994). b) Reconstruction of East Gondwana at ~150 Ma based on reconstructions from Gibbons et al. (2012), Bian et al. (2019) and Zhu et al. (2009). The Jurassic crust sliver (not to scale) was likely formed at the Argo Ridge when Argoland separated from East Gondwana. Locations of the Dronning-Maud Land and Ferrar LIP after Storey et al. (2013) and those of the Comei Igneous Province, Bunbury Basalts and Rajmahal Traps after Chen et al. (2021) and Zhu et al. (2009) (formed after 150 Ma) are also shown. The location of the hypothetical Exmouth mantle plume with the plume conduit outlined as stippled line and the minimum plume head outlined as dashed line based on assumptions of Rohrman (2015). GB = Gascoyne Block, WP = Wallaby Plateau, ZP = Zenith Plateau.

### 2.2. Major element analyses

Major element compositions of the glass samples were determined using a JEOL JXA 8200 electron microprobe at GEOMAR Helmholtz Centre for Ocean Research Kiel, Germany. Analytical conditions were 15 kV accelerating voltage, 6 nA current and 5 μm electron beam size. Details of the analytical procedure, standards used and data on long-term reproducibility of reference materials including high-Mg MPI-DING glasses are reported in Portnyagin et al. (2020). The glass compositions (Table S1) are averaged from 7 to 8 spots measured in 3 to 4 different glass chips. VG-2 glass (USNM 111240/52; Jarosewich et al., 1980) was analyzed as unknown in one series with the samples (Table S3). Typical uncertainty of the data for basaltic glasses estimated from long-term reproducibility of reference materials is ~2 rel.% for Si, Al, Mg, Ca, ~ 3–5 rel.% for Fe and Ti, 10 rel.% for Na, 15 rel.% for K and S, and ~30 rel.% for Mn and P (Portnyagin et al., 2020).

### 2.3. Trace element analyses

Trace element analyses were conducted using laser ablation inductively coupled plasma mass spectrometry (LA-ICP-MS) at the Institute of Geosciences, Kiel University, Germany. The analyses were performed using a QP-ICP-MS Agilent 7900 (DR30) and Agilent 8900 (ODP Site 765) and a Coherent GeoLas ArF 193 nm Excimer HD LA system operated with a fluence of 5–10 J $cm^{-2}$, at a repetition rate of 10 Hz and 60–160 μm ablation craters, and the ICP-MS was operated under standard conditions at 1500 W and optimized for low oxide formation (typically ThO/Th ≤0.4 %). A large volume ablation cell modified for rapid wash-out (Fricker et al., 2011) in a flow of He (0.7 l $min^{-1}$) with addition of 14 ml $min^{-1}$ $H_2$ was used and the carrier gas was mixed with Ar (~1 l $min^{-1}$) prior to introduction to the ICP-MS. Ten major elements (Si, Ti, Al, Fe, Mn, Mg, Ca, Na, K, P) and 46 trace elements were analyzed. Analyses included 20 s background (laser-off) and 40 s signal (laser-on) measurements. Dwell time for different isotopes varied from 5 to 20 ms depending on their abundance and one complete measurement cycle lasted 0.883 s. The calibration was based on SRM NIST612 glass standard (Jochum et al., 2011) and matrix corrected using KL2-G glasses (Jochum et al., 2006). Reference glasses BCR-2 G and GOR132-G were analyzed as unknown samples in one series with our glasses (Table S4). Initial data reduction was performed with Glitter software that included manual selection of integration windows and preliminary calibration (Griffin et al., 2008). The intensities corrected for background and averaged over the selected intervals were normalized to the intensity of $^{43}Ca$ isotope and converted to concentrations by matching the sum of major element oxides to 100 wt%. Analyses of the glasses (Table S1) are average compositions from 3 analyses in different glass chips. Typical uncertainty of the LA-ICP-MS data estimated from the reproducibility of reference materials (Table S4) is ≤5 rel.% (2 s) at element content ≥0.2 μg/g.

### 2.4. Volatiles

The CAMECA IMS 1270 secondary ion mass spectrometer (SIMS) at CRPG, Nancy, France was used to analyze $CO_2$, $H_2O$, Cl, S and F in the glass samples (Table S1). A set of reference MORB glasses and nominally volatile-free olivine (ALV981-R23, ALV519-4-1, 30-2, 40-2, KL2-G, CY8406-02 and San Carlos olivine) were used to define calibration lines. Analytical details are provided by (Sobolev et al., 2016). Typical uncertainty of the SIMS data is ≤10 rel.% for $H_2O$, Cl, S and 15 rel.% for $CO_2$.

### 2.5. Radiogenic isotope analyses

Sr-Nd-Pb-Hf isotope analyses of glass sample SO199-DR30-1A (Table S1) were conducted at GEOMAR from 2008 to 2011 along with samples from the CHRISP using the same analytical procedures as described in Hoernle et al. (2011b). New analyses of samples DR30-2 and DR30-3 were processed at GEOMAR on a Thermo Scientific TRITON+ thermal ionization mass spectrometer (TIMS) for Sr, Nd and Pb and on a NEPTUNE+ MC-ICP-MS for Hf in 2021. Sr and Nd were collected in multi-dynamic and Pb and Hf in static collector mode. Prior to digestion, ~200 mg of fresh glass chips were leached in 2 N HCl at 50 °C for 0.5 h and then triple rinsed in 18.2 MΩ cm water. Sample dissolution and Sr-Nd-Pb element chromatography followed established standard procedures (Hoernle et al., 2008) with a modified Sr clean-up using Sr-Spec microcolumns. Hf was separated on the cation exchange column (AG50W-X8, 100–200 mesh) over the first 2 ml using a 1.5 M HCl media followed by a Hf clean-up using 0.2 ml of TODGA resin (50–100 μm; DN-B10-S TRISKEM®) after Connelly et al. (2006). Total chemistry blanks were <100 pg for Sr, <50pg for Nd, Hf and <30 pg for Pb and therefore considered negligible relative to the amount of the processed samples. Sr and Nd isotope ratios were mass-bias corrected within run to $^{86}Sr/^{88}Sr = 0.1194$ and $^{146}Nd/^{144}Nd = 0.7219$, respectively. Analyses of reference materials were carried out along with the samples and produced $^{87}Sr/^{86}Sr = 0.710250 \pm 0.000009$ (2σ standard deviation (2SD); n = 8) for NBS987 and $^{143}Nd/^{144}Nd = 0.511850 \pm 0.000006$ (2SD; n = 7) for La Jolla. Pb isotope ratios were determined using the Pb double-spike (DS) technique described in Hoernle et al. (2011a). Since instrument installation in 2014, long term DS-corrected values for NBS981 are $^{206}Pb/^{204}Pb = 16.9408 \pm 0.0019$, $^{207}Pb/^{204}Pb = 15.4974 \pm 0.0019$ and $^{208}Pb/^{204}Pb = 36.7206 \pm 0.0050$ (2SD; n = 228). Our in-house SPEX CertiPrep® Hf ICP standard solution (lot #9) yielded $^{176}Hf/^{177}Hf = 0.282170 \pm 0.000005$ (2SD; n = 36) corresponding to $^{176}Hf/^{177}Hf = 0.282163$ for JMC475. USGS reference material BCR-2 was processed along with the samples and agrees well with the previously published data (Table S5).

## 3. Results

Volcanic glasses separated from the margins of four fragments of pillow lavas dredged at station SO199-DR30 were analyzed for the content of major and trace element, volatiles ($H_2O$, $CO_2$, F, S, Cl), and Sr-Nd-Hf-Pb isotope ratios. In the course of this study, we also obtained previously not available high quality major and trace element data for four glass samples recovered at ODP Leg 123 cores 765C and 765D in the Argo Abyssal Plain (Ishiwatari, 1992; Ludden and Dione, 1992). All geochemical data from this study are reported in Table S1.

The DR30 rocks are aphyric basalts except for the presence of rare, small olivine phenocrysts. The analyzed DR30 volcanic glasses have identical compositions within analytical uncertainty. The glasses display a very primitive low-K tholeiitic composition with $SiO_2$ ~48 wt%, $Na_2O$ ~2 wt% and $K_2O$ ~0.06 wt%, and have a very high MgO content of ~10.5 wt%, which are the highest reported for MORB glasses globally (Fig. 2). The glasses are also relatively rich in total FeO (~9.8 wt%) and thus their Mg# ~65.4 mol.% is not extremely high, within the range of more typical MORB glasses with 8.5–9 wt% MgO. Eruption temperature estimated with COMAGMAT (Ariskin and Barmina, 2004) is 1250 °C, and equilibrium olivine is $Fo_{87}$ at $FeO/(FeO+Fe_2O_3)$ ~ 0.9 in melt. Volatile contents are in the lowermost range reported for MORB (Dixon et al., 2002) with $H_2O = 0.174$ wt%, $CO_2 = 188$ μg/g, S = 940 μg/g, Cl = 37 μg/g and F = 110 μg/g (average of 6 analyses). $H_2O/Ce$ ~360 (weight ratio) in DR30 glasses are higher than in typical MORB glasses and similar to "wet-EM" (enriched mantle)-type MORB glasses from regions of plume-ridge interaction (Dixon et al., 2017) and some segments along the Southwest Indian Ridge (Wang et al., 2021).

Jurassic MORB glasses from ODP Leg 123 Site 765 in the Argo Abyssal Plain analyzed in this study have relatively low MgO = 7–7.5 wt % and major element contents that are typical for evolved Fe-rich MORB compositions (Fig. 2). Modeling shows that DR30 and Site 765 glasses cannot be genetically related by crystal fractionation. A distinctive feature of the Site 765 glasses is that they have high FeO and low $Al_2O_3$ contents marginally outside the MORB range at a given MgO content

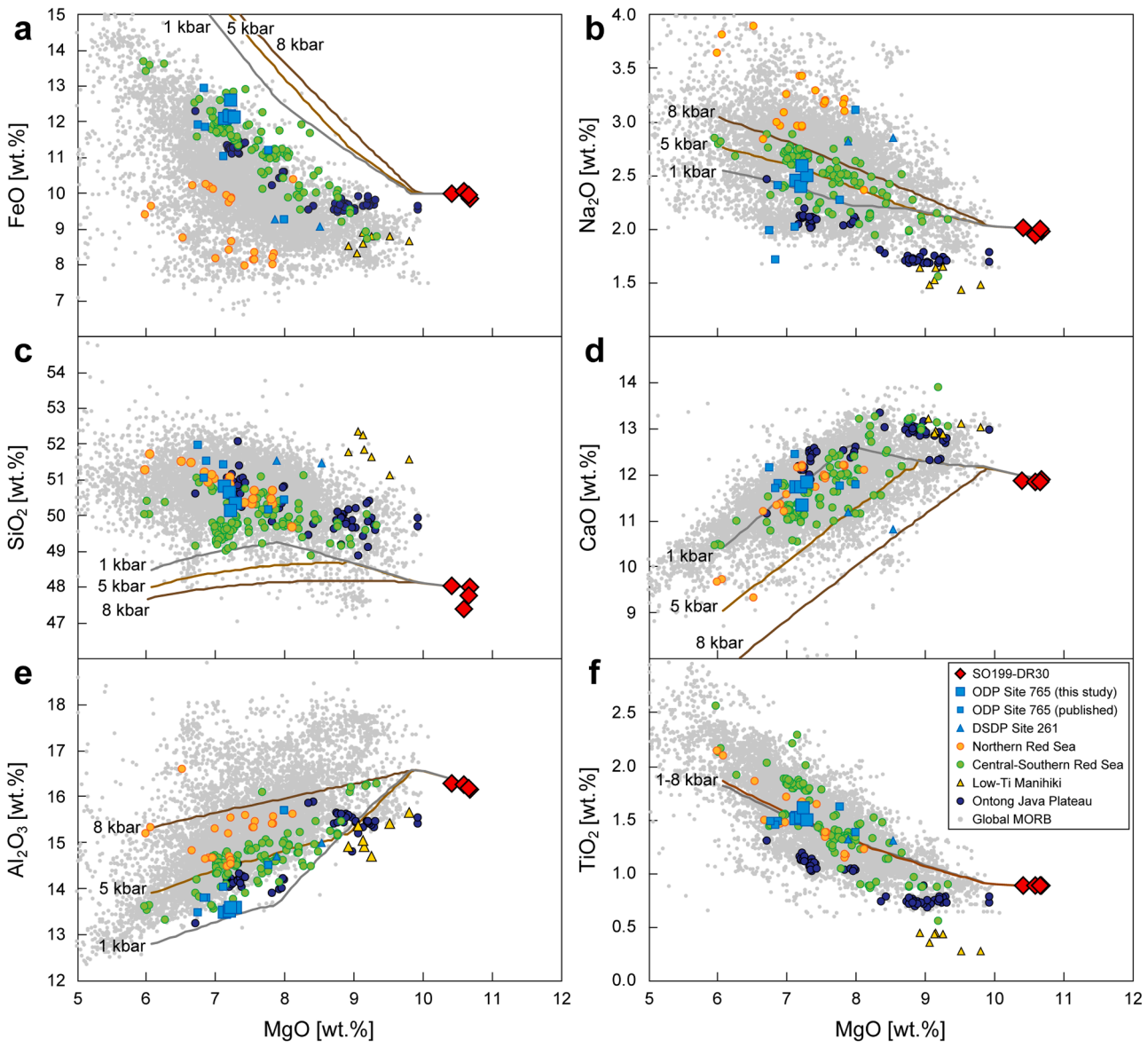


**Fig. 2.** Major elements in Jurassic Indian MORB. Major element compositions of SO199-DR30 glasses in comparison with Argo Abyssal Plain glasses from ODP Sites 765D and 765C (small symbols: Ishiwatari, 1992, large symbols: this study), DSDP Site 261 (Frey et al., 1977), global MORB glasses (Melson et al., 2002), northern (latitude >25°N), central and southern (latitude <25°N) Red Sea glasses (van der Zwan et al., 2015; Jenner and O'Neill, 2012; Ligi et al., 2012), northern Red Sea glasses (Haase et al., 2000), Ontong Java Plateau glasses (OJP; Roberge et al., 2004) and low-Ti Manihiki Plateau glasses (Golowin et al., 2017). Trends of melt evolution through fractional crystallization from parental DR30 glass were calculated using the Comagmat-3.72 software (Ariskin and Barmina, 2004) for 1, 5 and 8 kbar crystallization pressure and oxygen fugacity at FMQ.

(Fig. 2a and e), indicating nearly anhydrous high-temperature parental melts (Langmuir et al., 1992; Wang et al., 2022). The major element compositions of ODP Site 765 glasses are close to Fe-rich basaltic glasses from the central and southern parts of the Red Sea (Fig. 2).

In comparison to normal (N-)MORB, DR30 glasses 1) have similar contents of heavy rare earth elements (HREEs; e.g., Yb), Y and Th, 2) are up to two times more depleted in most medium (e.g., middle REEs, Ti, Zr) and highly (U, Nb, light REEs) incompatible elements, and 3) are slightly enriched in the most incompatible elements Rb and Ba (Fig. 3). Therefore, the incompatible elements form spoon-shaped patterns on multi-element diagrams. Such patterns are atypical for MORB but found in some rocks from the Nereus Deep in the central Red Sea (Altherr et al., 1988; Jenner and O'Neill, 2012) and from the Suvorov and Danger Islands Troughs in the Manihiki Plateau (Golowin et al., 2017) (Fig. 3). A distinctive feature of the DR30 glasses is significantly lower Dy/Yb (~1.2) than typical for primitive MORB (average Dy/Yb ~ 1.5 at MgO>8.5 wt%) (Fig. 4a). Comparably low Dy/Yb were also reported for low-Ti Manihiki glasses (Golowin et al., 2017). However, unlike the Manihiki glasses, DR30 glasses have 2.5× higher contents of heavy REE and Y.

ODP Site 765 glasses have compositions close to typical N-MORB with the contents of the most incompatible elements (Rb, Ba, Th, U, Nb, Ta) more depleted and Ti, Y and HREE contents more enriched than in average primitive N-MORB and SO199-DR30 glasses (Fig. 3). Dy/Yb ratio in the Argo Basin glasses is very similar to that in N-MORB and significantly higher than in SO199-DR30 samples (Fig. 4a).

In terms of radiogenic isotope ratios, DR30 glasses show an enriched, DUPAL-like, signature with average initial $^{206}Pb/^{204}Pb$ = 18.30, $^{207}Pb/^{204}Pb$ = 15.54, $^{208}Pb/^{204}Pb$ = 38.36, $^{87}Sr/^{86}Sr$ = 0.70416, $^{143}Nd/^{144}Nd$ = 0.51266, and $^{176}Hf/^{177}Hf$ = 0.28301 (calculated at 155.6 Ma; see Fig. 5 caption for details) and they overlap or are slightly more enriched than the enriched part of the Indian MORB field (Fig. 5).

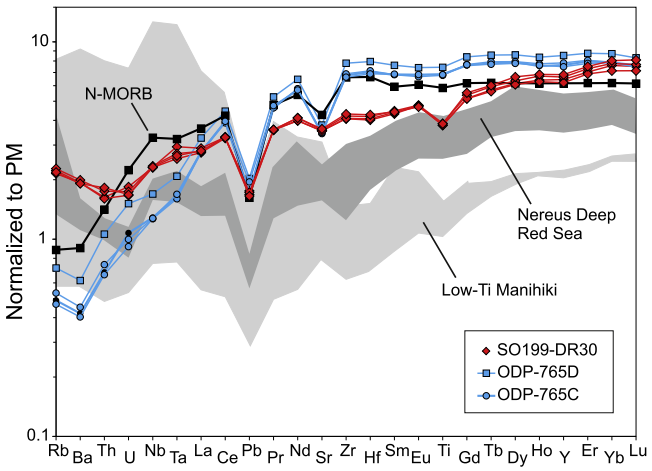


**Fig. 3.** Systematics of incompatible trace elements. Trace element compositions of Jurassic Indian MORB glasses (dredge site SO199-DR30 and ODP Sites 765D and 765C) compared with primitive N-MORB (Sun and McDonough, 1989), low-Ti Manihiki (Golowin et al., 2017) and basaltic glasses from the Nereus Deep, Red Sea (Altherr et al., 1988; Jenner and O'Neill, 2012). Normalization to primitive mantle (PM; Sun and McDonough, 1989).

In general, these compositions are typical for the Christmas Island Seamount Province (CHRISP) in the eastern Indian Ocean. Published data from ~155 Ma old ODP Site 765 and ~152 Ma old DSDP Site 261 samples from the Argo Abyssal Plain (Fig. 1a) also largely plot within the Indian MORB field but at lower initial $^{206}Pb/^{204}Pb$ ratios than the DR30 glasses, and in terms of Sr isotope ratios, they more closely resemble Pacific MORB (Fig. 5).

## 4. Discussion

### 4.1. Hybrid mantle source and its pre-conditioning

The compositions of glasses from the sliver of Jurassic oceanic crust attached to the Investigator Ridge are unusual in global MORB systematics and may imply specific source composition and/or conditions of mantle melting. On the one hand, the glasses have high CaO (~11.9 wt%), 1000*Mn/Fe ~ 18.8 and 1000*Zn/Fe~10.2 that imply an origin from a predominantly peridotite, similar to depleted MORB mantle (DMM) or primitive mantle (PM) source (e.g., Herzberg and Asimow, 2008; Le Roex et al., 2010). On the other hand, systematics of incompatible trace elements in DR30 glasses are not consistent with the simple model of one-stage melting of depleted or slightly enriched peridotite source (Fig. 4). The contents of HREE and Y are much higher, and Dy/Yb ratio is much lower in DR30 glasses and their potential parental melts as calculated in PRIMMELT3 software (Herzberg and Azimow, 2015) in comparison with the expected products of one-stage mantle peridotite melting at $T_P$ ranging from 1340 to 1460 °C (Fig. 4a). With respect to low Dy/Yb, DR30 melts are similar to low-Ti melts from the Manihiki Plateau, which were explained by two-stage mantle peridotite melting, first at a mid-ocean ridge and later as part of a mantle plume (e.g., Golowin et al., 2017). At comparably low Dy/Yb ratios, an important difference to the Manihiki magmas is, however, the high absolute content of HREEs and Y in the DR30 melts (Figs. 3 and 4). Inverse modeling of the DR30 source composition, assuming 10–30 % degrees of melting, yields 4.5–8.5 μg/g Y in the source, which is higher than in primitive or depleted mantle (3.2–4.3 μg/g, Workman and Hart, 2005; Sun and McDonough, 1989) and their melting residues in either the garnet or spinel stability fields (Fig. 4b). These observations imply that parental DR30 magmas cannot originate from DMM-like peridotite mantle or its residues. The mantle source of DR30 should have significantly higher Y and HREE contents compared to the prevailing DMM-like mantle

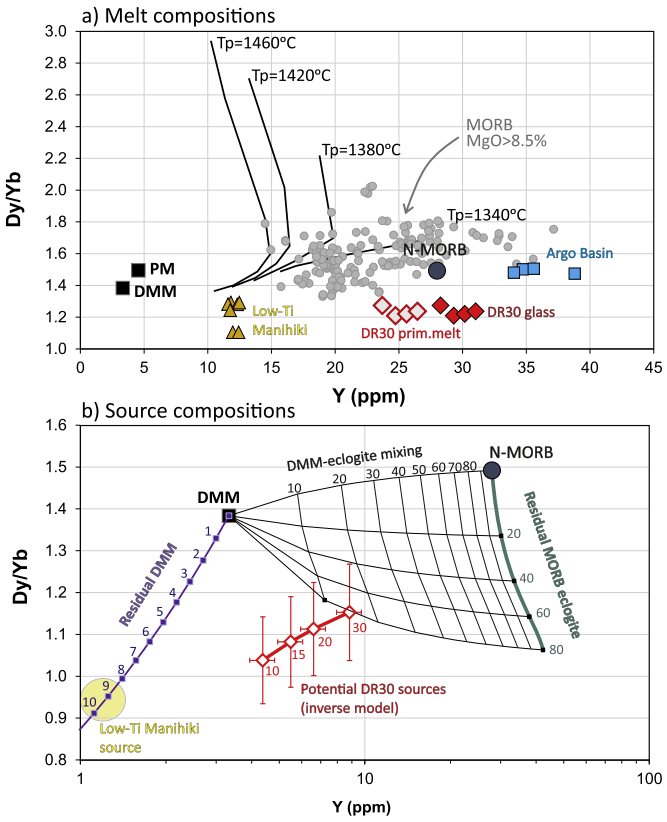


**Fig. 4.** Systematics of Y and Dy/Yb in Jurassic Indian MORB and its potential sources.
a) Compositions of SO199-DR30 and Argo Basin glasses in comparison with primitive MORB compositions with MgO >8.5 wt% (Gale et al., 2013; Jenner and O'Neill, 2012), average primitive N-MORB (Sun, McDonough, 1989), low-Ti Manihiki glasses (Golowin et al., 2017), primitive mantle (PM; Sun and McDonough, 1989) and depleted MORB mantle (DMM, Workman and Hart, 2005). Solid lines show trajectories of the composition of accumulated partial melts from DMM source with different potential temperatures ($T_p$) as calculated with the OBS-1 software (Kimura and Kawabata, 2015). SO199-DR30 glasses have distinctively low Dy/Yb (similar to that in low-Ti Manihiki glasses) and high Y in comparison to all primitive MORB. Agro Basin glasses have compositions corresponding to evolved N-MORB.
b) Potential source compositions for SO199-DR30 primary melts. The source compositions were calculated for degrees of melting of 5, 10, 15, 20 and 30 % using equations of batch partial melting and bulk partition coefficients for shallow DMM melting after Workman and Hart (2005). Uncertainty of Dy/Yb and Y content in the DR30 primary melts is assumed to be 10 rel.%. Residual DMM compositions after 1–10 % fractional melting were calculated using bulk partition coefficients after Workman and Hart (2005). Partial melting of N-MORB eclogite and its residual compositions after 20 to 80 % melting were calculated using the OBS-1 software (Kimura and Kawabata, 2015). Residual DMM after 9–10 % melting is appropriate source for low-Ti Manihiki magmas (Golowin et al., 2017), whereas DR30 melts require source with Dy/Yb lower than in DMM and significantly enriched in Y, which can be unmelted DMM mixed with 10–20 % residual eclogite.

peridotites.

Thus, a viable model for the origin of parental DR30 magmas should explain their Fe-rich primitive composition, high CaO, Mn/Fe and Zn/Fe within the range of peridotite-derived magmas, undepleted HREE abundances and, on the contrary, very low Dy/Yb, suggesting previous mantle melting.

In order to explain these unusual and in part seemingly incompatible compositional features, we propose that the mantle source of the DR30 melts might be of a hybrid nature, initially composed of a mixture of mantle peridotite and mafic eclogite and thus was more enriched in all incompatible elements compared to DMM. A possible model explaining

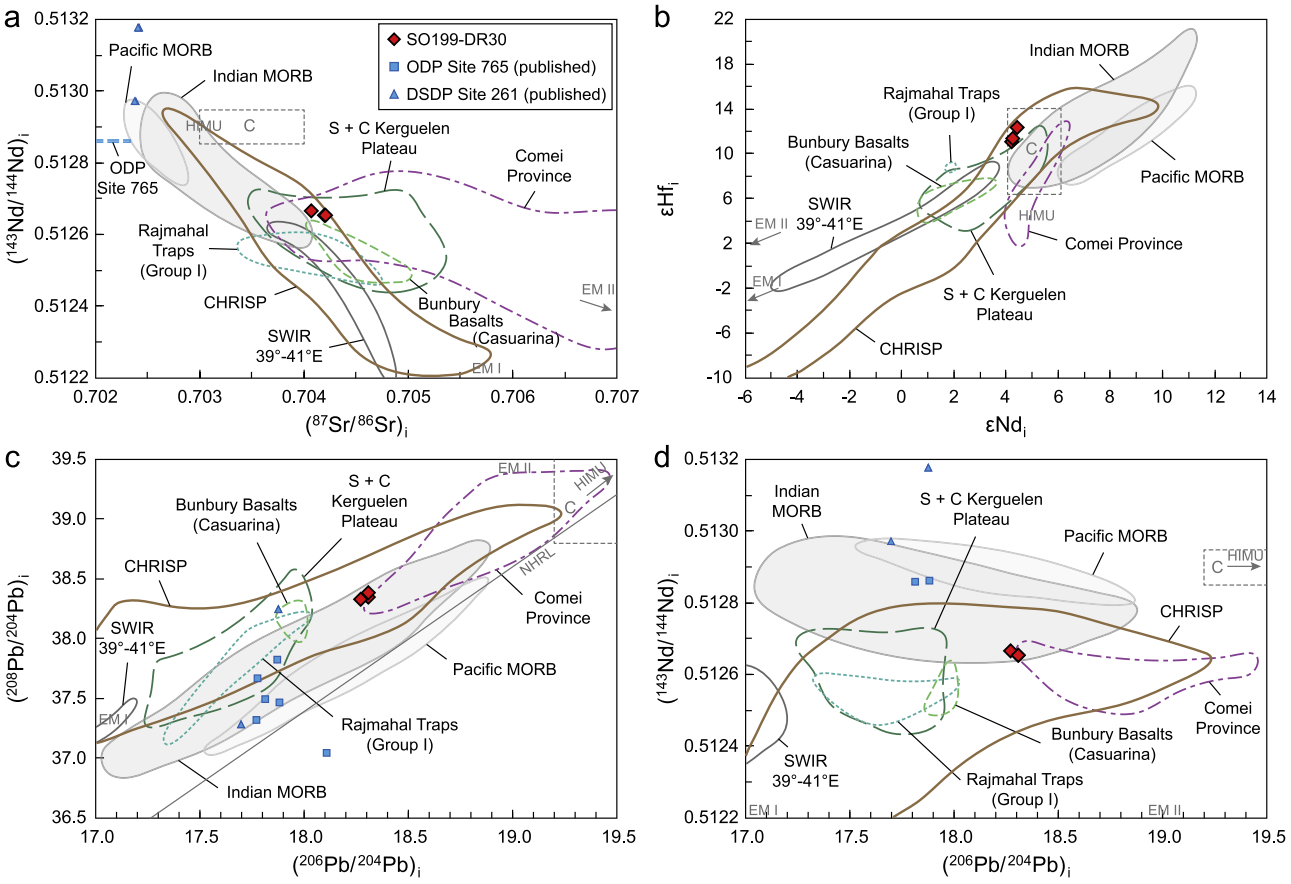


**Fig. 5.** Radiogenic isotope compositions. Initial **a** $^{87}Sr/^{86}Sr$ versus $^{143}Nd/^{144}Nd$, **b** ƐNd versus ƐHf, **c** $^{206}Pb/^{204}Pb$ versus $^{208}Pb/^{204}Pb$ isotope and **d** $^{206}Pb/^{204}Pb$ versus $^{143}Nd/^{144}Nd$ diagrams showing that the DR30 glass samples are more enriched than Pacific MORB but plot within or near the enriched part of the Indian MORB field (Pacific and Indian MORB data: PetDB at http://www.earthchem.org/petdb) and overlap with the composition of rocks from the Christmas Island Seamount Province (CHRISP) in the eastern Indian Ocean (Hoernle et al., 2011b). They also lie near (c and d) or overlap with (a) the depleted samples from the Comei Province in SE Tibet (Chen et al., 2021; Xia et al., 2014; GEOROC at http://georoc.mpch.gwdg.de/georoc/), whereas samples from the Bunbury Basalts (Casuarina Group), Rajmahal Traps and Southern and Central (S + C) Kerguelen Plateau (data from GEOROC at http://georoc.mpch.gwdg.de/georoc/) have more unradiogenic $(^{206}Pb/^{204}Pb)_i$ (c and d) and only the Kerguelen field overlaps with the DR30 glasses in a. ODP Site 765 (Ludden and Dionne, 1992) and DSDP Site 261 (Weis and Frey, 1996) samples generally resemble Indian MORB. The initial isotopic compositions from the Jurassic glasses have been calculated to 155 Ma using the measured parent/daughter ratios; the reference data have been calculated to their respective ages using measured parent/daughter ratios and were then projected to a common age of 155 Ma using estimated source parent/daughter ratios (Willbold & Stracke, 2006; Workman & Hart, 2005; Stracke et al., 2003).

the key geochemical features of the DR30 source is illustrated in Figs. 4b and 6.

We propose that the mantle source parental to primary DR30 melts could be initially composed by ~70-80% depleted mantle and 20-30% eclogite of N-MORB composition. Modeling using the OBS-1 software (Kimura and Kawabata, 2015) shows that at potential mantle temperature of ≥1350°C and at pressures of 3-3.5 GPa the pyroxenite could be melted up to at least ~50%, whereas depleted peridotite would not melt or only melt to a few degrees depending on the mantle $T_P$. Provided that the first stage melting took place under ~100 km thick continental lithosphere, it would limit further mantle upwelling and melting of depleted peridotite. As a result of this incipient melting, the eclogite component becomes strongly depleted in highly incompatible elements but enriched in moderately incompatible elements such as the HREEs and becomes a very low Dy/Yb, which are retained and fractionated in the source by residual garnet. Accordingly, the bulk source composition comprised by ~85% DMM and 15% residual eclogite becomes enriched in HREEs and remains similar to DMM for the more incompatible elements (Figs. 4b and 6). Melting of this source to ~20% can explain reasonably well the abundances of moderately incompatible elements including relatively high contents of HREE, low Dy/Yb and pronounced depletion in MREE, Zr and Hf compared to typical N-MORB (Fig. 3). The possible presence of residual eclogites in the source of DR30 magmas does not contradict high CaO, Mn/Fe and Zn/Fe in the melts, because residual eclogites should evolve to higher than initial CaO, Mn/Fe and Zn/Fe, and their second-stage melts should not be significantly different from peridotite-derived melts in terms of these compositional proxies.

Slight enrichment of the DR30 melts in the most incompatible elements compared to N-MORB (Fig. 3) suggests that their source was slightly re-fertilized by enriched melt before it was involved in a second partial melting event. For example, a close fit for incompatible elements is obtained by 0.5% metasomatism of the depleted mantle by OIB-like enriched melt. The relative contribution from the enriched component is estimated to be 20-50% for Hf, Nd, Sr, and Pb (ordered by increasing contribution from the enriched component), which should have a pronounced effect on their isotope ratios and can explain the apparent paradox of the enriched isotope and depleted trace element DR30 compositions.

Pearce (2005) noted that the geochemical trends of the Red Sea basalts are different from simple source and/or magma mixing trajectories. Instead, he proposed that their compositional array extending from enriched to very depleted compositions can be explained by "mantle preconditioning" - the process of gradual modification of lithologically heterogeneous (e.g., peridotite with pyroxenite veins) mantle by extraction of small degree melts as the mantle flows to the site of extensive magma generation under a mid-ocean ridge.

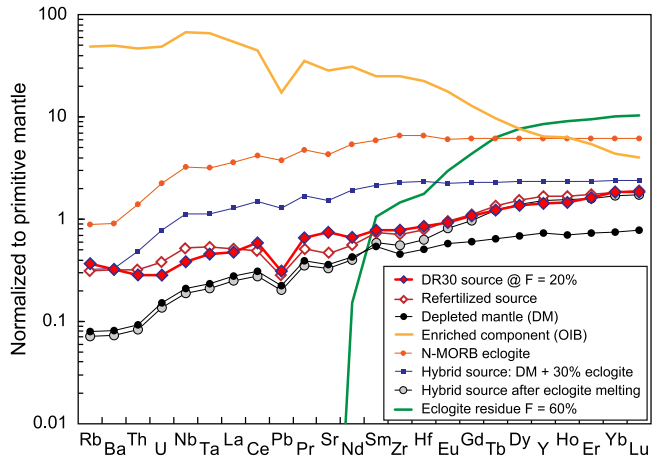


**Fig. 6.** Forward and inverse modeling of hybrid source composition. The forward model of the DR30 source composition (red open diamonds) includes the following steps: 1) mixing 70 % DMM with 30 % N-MORB-like eclogite, 2) melting of eclogite to 60 % and calculation of new hybrid source composed by DMM and 12 % residual eclogite, 3) addition of 0.5 % OIB melt to the hybrid depleted source. Inverse model of the DR30 source composition (red diamonds with blue outline) assumes the origin of DR30 primary melts by 20 % melting of spinel peridotite. The problem is solved when good agreement between the forward and inverse models is achieved. The OBS-1 model was used for modeling of eclogite melting (Kimura and Kawabata, 2015). Data sources: depleted mantle peridotite (DM) and bulk partition coefficients after Workman and Hart (2005), N-MORB eclogite after Kimura and Kawabata (2015), enriched component - ocean island basalt (OIB) after Sun and McDonough (1989). Normalization to primitive mantle after Sun and McDonough (1989).

In essence, this model is very similar to what we propose in our study, and DR30 glasses reveal compositional similarity with some rocks from the Red Sea deeps (Figs. 2 and 3). Compositional similarity with Fe-rich variably enriched MORB from the Red Sea has also been pointed out for the ODP Site 765 basalts (Ludden et al., 1992b; this study) and rocks dredged at the SW corner of the Exmouth Plateau and the margin of the Scott Plateau adjacent to the Argo Basin (Crawford and von Rad, 1994). Based on this similarity, we propose that the mantle preconditioning can be a characteristic process associated with continental breakup. This process leads to the formation of a distinct type of MORB-like magmas as illustrated by the basalts from the Red Sea and also from the sliver of Jurassic seafloor in the eastern Indian Ocean studied here.

### 4.2. *Effect of peridotite Mg# on estimates of mantle potential temperature*

In the previous section, we showed that the incompatible trace element contents in DR30 melts cannot be explained by one- or two-stage melting of DMM or PM-like peridotitic sources. Instead they require the presence of low Mg# eclogite or pyroxenite in the source. We also argue that identification of the residual eclogite lithology in the source of mantle magmas can be problematic using common geochemical ratios, such as Mn/Fe and Zn/Fe ratios in primitive rocks (Herzberg and Asimow, 2008; Le Roex et al., 2010). It is thus important to evaluate the potential effect of the presence of a residual eclogite in mantle peridotite on the estimates of mantle potential temperatures. This effect should arise from the lowering of the bulk mantle Mg#, decreasing liquidus Fo-number of olivine and MgO in the primary melts.

Firstly, we estimate the maximum $T_P$ assuming pure peridotite source composition. Our calculations using the PRIMELT3 model (Herzberg and Asimow, 2015), $Fe^{2+}/Fe_{Total}$=0.9, peridotite composition with FeO=8.0 wt% and MgO=38.1 wt% (Mg# = 89.5 mol.%), and applying an accumulated fractional melting model, yielded MgO contents of the primary magma of 16.0–16.3 wt% in equilibrium with forsterite $Fo_{91.3}$, and melt fractions of 17–20 % at a potential mantle temperature ($T_P$) of ~1465 °C (Table S2, Fig. 7a). A similar estimate of

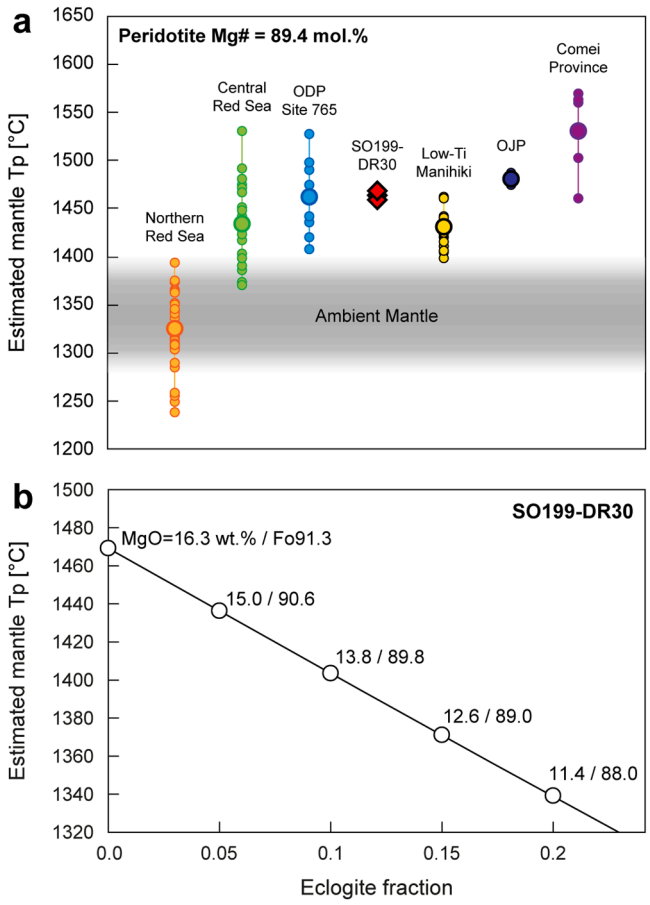


**Fig. 7.** Mantle potential temperatures ($T_P$) for Jurassic Indian MORB. **a.** $T_P$ for primary melts of DR30 glasses, low-Ti series from Manihiki plateau (Golowin et al. 2017), and Ontong Java Plateau (OJP; Roberge et al., 2004) were calculated using the PRIMELT3 MEGA.xlsm software (Herzberg and Asimow, 2015), assuming accumulated fractional melting and high-Mg# pure peridotite composition. $T_P$ for the Comei Province are from Chen et al. (2021), Wang et al. (2018) and Xia et al. (2014). $T_P$ for the northern Red Sea MORB were calculated from $Fe_{8.0}$ and $Na_{8.0}$ (Mg# = 0.63–0.67), for ODP Site 765 - from $Fe_{8.5}$ and $Na_{8.5}$ (Mg# = 0.59–0.60), and for the central Red Sea - from FeO and $Na_2O$ in glasses with MgO>8.5 wt% (Mg#>0.6) using equations from Kelley et al. (2006). The same approach applied to uncorrected DR30 glasses returns $T_P$ = 1460 °C, which is very similar to the calculations using PRIMELT3. Large dots depict average $T_P$.
**b.** Effect of low-Mg# eclogite admixture to mantle peridotite on the estimates of $T_P$, MgO in primary melt and liquidus olivine composition for DR30 magmas. Peridotite composition with MgO=38.12 wt% and FeO=8.02 wt% is after Herzberg and Asimow (2015). Eclogite composition with MgO=11.9 wt% and FeO=12.5 wt% is residual assemblage after 51 % melting at 1500 °C and 3 GPa comprised by 37 % garnet, and 63 % clinopyroxene (Kogiso and Hirschmann, 2006). Calculations were performed in PRIMELT3 MEGA.xlsm software (Herzberg and Asimow, 2015).

$T_P$ ~ 1460 °C is obtained using Na–Fe systematics in peridotite-derived melts in equilibrium with olivine $Fo_{90}$ (Kelley et al., 2006). These results indicate melting of a mantle source that could be more than 100 °C hotter than expected for the ambient upper (MORB) mantle source with $T_P$ of ~1350 °C on average (Herzberg et al., 2007). The estimated mantle potential temperature is only slightly lower than that calculated for the Ontong Java Plateau (average $T_P$ = 1481 °C) and slightly higher that calculated for low-Ti volcanic rocks from Manihiki Plateau (average $T_P$=1432 °C) using the same initial conditions (Golowin et al., 2018; Fig. 7a).

Herzberg and Asimow (2015) did not recommend to change Mg# of mantle peridotite for PRIMELT3 calculations because a fully

quantitative evaluation of the estimated $T_P$ and potential variability in the source Mg# is not possible with the presently available experimental data. However, semi-quantitative prediction of the effect of peridotite Mg# on the estimated $T_P$ should be correct. As noted above, our calculations use typical peridotite composition with Mg# = 89.5 mol.% (FeO=8.0 wt% and MgO=38.1 wt%), adopted by Herzberg and Asimow (2015) for calculations with PRIMELT3 software, and residual eclogite after 60 % melting at 1500 °C and 3 GPa with Mg#=62.9 mol.% (MgO=11.9 wt% and FeO=12.5 wt%) (Kogiso and Hirschmann, 2006). Our results show that addition of ~15% of residual eclogite decreases mantle Mg# to 86.8 mol.%. In the case of DR30 primary melts, the liquidus olivine Fo-number decreases to 89 mol.% and predicted MgO in primary melt is 12.6 wt% (Fig. 7b), with the estimated mantle potential temperature $T_P$ being 1371 °C, or ~100 °C lower compared to pure peridotite melting.

Thus, we propose that the estimated $T_P$~1465 °C for the case of high-Mg# peridotite melting is likely a maximum possible potential temperature for the DR30 mantle source. The magmas could originate from significantly colder mantle depending on the amount of recycled low-Mg# material in the source. If a relatively large amount of pyroxenite/eclogite (10–15 %) is present, as we suggest in our study, the $T_P$ can be similar to that of the ambient mantle (Fig. 7b). A relatively high $T_P$ estimated for evolved Argo Basin MORB (Fig. 7a) should also be considered to be a maximum value, due to large backward correction of the glass composition to the point where plagioclase joined olivine on the MORB cotectic, which significantly affects the estimated FeO in the primary melts and accordingly $T_P$ estimate (e.g., Herzberg et al., 2007).

The above results show the necessity of a very careful examination of major and also trace element composition of primitive basalts for their consistency with regard to the presence of low Mg# recycled material in mantle sources. The underestimation of involvement of low Mg# crustal material and subsequent overestimation of the source Mg# may result in unrealistically high $T_P$ estimates and thus the conclusion for the involvement of a mantle plume with excess temperature in generating the magmatism (e.g., Herzberg et al., 2007). In the case of the Jurassic Indian MORB, we argue that their Fe-rich primitive compositions may not require involvement of a hot mantle plume in agreement with some previous studies (Crawford and von Rad, 1994; Ludden and Dionne, 1992).

### 4.3. Possible geodynamic scenario

The hypothetical geodynamic scenario for the magmatism in the eastern Indian Ocean preceeding and following the Gondwana breakup is illustrated in Fig. 8. During the first stage, we propose that mantle upwelling brings recycled oceanic crust to the base of continental lithosphere, where this crustal material melts to produce small volume magmatism forming dykes, sills and small volcanoes. We propose that the upwelling mantle could contain up to 30 % N-MORB-like eclogite (Fig. 8a). This amount of dense eclogite appears to be too large to be entrained in steadily upwelling mantle with little or no excess temperature (e.g. Sobolev et al. 2011). Nevertheless, we argue that a mantle plume does not need to be involved in the origin of the Jurassic Indian MORB. A plausible alternative to the plume hypothesis for transporting dense eclogites to the shallow depths can be a short-lived upwelling in response to an avalanche of subducted slab material from the transition zone to the lower mantle (Korenaga, 2004). During the second-stage (Fig. 8b), continental breakup allows residual eclogite and peridotite to upwell and melt by decompression, possibly assissted by convection (e.g., King and Anderson, 1998; Hoernle et al., 2011b).

Ligi et al. (2011) have shown that eruption rate, spreading rate, magnetic intensity, crustal thickness and degree of melting of the sub-axial upwelling mantle beneath a spreading center are highest in the very initial phases of oceanic crust formation directly following continental breakup at both Thetis and Nereus Deeps in the Red Sea. The authors explained these observations by an initial pulse of active edge-driven subrift mantle upwelling triggered by a sharp horizontal thermal gradient between cold continental lithosphere and hot asthenosphere. As the thermal gradient weakens with widening of the oceanic rift, the initial active pulse of seafloor spreading evolves into more passive crustal accretion, with slower spreading and along axis rift propagation. The remarkably close compositional similarity of the Red Sea basalts and the Jurassic Indian MORB (Figs. 2 and 3) strongly supports the model of Ligi et al. (2011) as a viable alternative to the mantle plume hypothesis and explains major compositional features of Jurassic Indian MORB such as 1) a relatively high degrees of melting, 2) the presence of mafic eclogite/pyroxenite in the mantle source, and 3) late stage involvement of an enriched component of likely continental provenance (SCLM and/or lower crust). Our results are in accord with

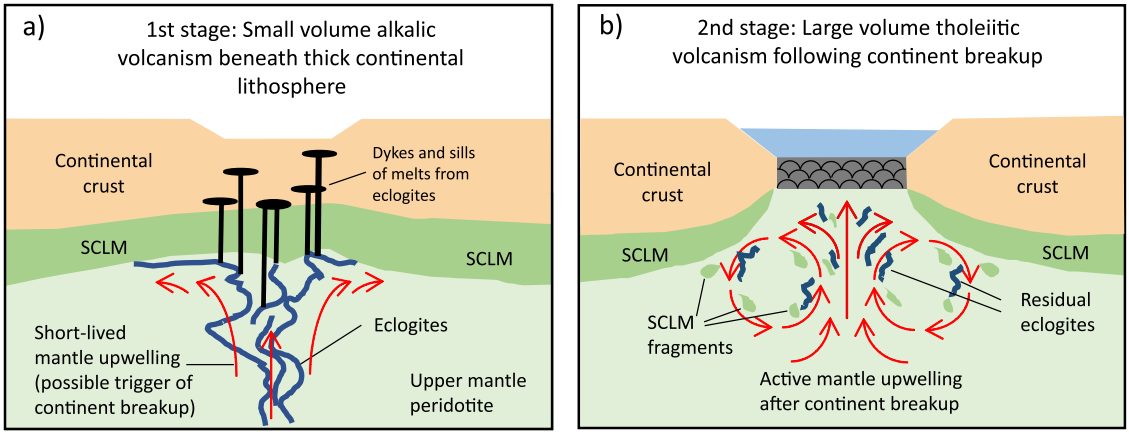


**Fig. 8.** Possible geodynamic scenario of two-stage mantle melting at breakup of a continent. During the first stage (a), partial mantle melting (pre-conditioning) takes place underneath thick continental lithosphere. It involves extensive melting of fertile eclogite embedded in a depleted peridotite matrix. Dense eclogites were possibly upwelled to the base of continental lithosphere by a mantle avalanche event (e.g. Korenaga, 2004). Locally the amount of eclogites could be large, as required by our geochemical modeling, but for the bulk mantle the amount likely does not exceed a few percent. During the second, main stage (b), as the continent breaks apart allowing mantle to upwell to shallow depths, enhanced by small-scale convection. Convection is induced at the continental edges due to sharp thermal gradient resulting in melting of undepleted peridotite enclosing eclogite residues after the initial melting stage. Eroded and delaminated fragments of enriched subcontinental lithospheric mantle (SCLM) are also involved in the mantle melting during this stage, which explains enrichment of the most incompatible elements and enriched Sr–Nd–Pb isotope signature of magmas.

those of Ligi et al. (2011; 2012) and suggest that the proposed scenario can offer a general mechanism of initial oceanic crust accretion immediately after continental break up.

## 5. Conclusions

A geochemical study of Jurassic ~155 Ma MORB volcanic glasses from the Investigator Ridge and Argo Abyssal Plain, eastern Indian Ocean produced the following major results:

1) The Jurassic glasses from the Investigator Ridge have the highest MgO (~10.6 wt%) contents found in mid-ocean ridge basalts thus far, as well as high FeO (~9.8 wt%). The glasses exhibit strong depletion in moderately incompatible elements such as middle REE, Zr, Hf, and Ti, compared to the less incompatible heavy REE and Y, and more incompatible elements, such as Rb, Ba, and Th. The trace element characteristics imply multi-stage mantle processing prior to a major melting event under a young ocean basin.
2) The model to reconcile major and trace element systematics of the Jurassic magmas suggests a two-stage melting scenario of a hybrid source comprising initially peridotite and large amounts (up to 30 %) recycled oceanic crust. The first-stage melting occurs under thick continental lithosphere and results in extensive melting of the eclogitized oceanic crust. During the second-stage, the hybrid source enriched in HREE – elements hosted in residual eclogitic garnet – melts to produce MORB-like parental magmas of the incipient oceanic magmatism.
3) Sr–Nd–Pb–Hf isotopic compositions of the Jurassic Indian MORB most closely align with those of the Christmas Island Seamount Province located just to the north of the DR30 sampling site. We propose the origin of this enriched signature via interaction of highly depleted partial mantle melts with continental lithosphere or recycled fragments of continental lithosphere in the upper mantle as argued previously for the origin of non-plume related magmatism of the Christmas Island Seamount Province. Argo Basin basalts tap highly depleted DMM-like mantle.
4) A deeply-sourced hot mantle plume is not necessarily required to explain the origin of the Jurassic Indian MORB. Instead, short-lived active upwelling of hot and lithologically heterogeneous mantle triggered by continental breakup, which was also proposed to explain intense volcanism at the initial opening of the Red Sea, can also provide a plausible explanation for the immature magmatism in the eastern Indian Ocean and can be considered as a valid mechanism of initial oceanic crust accretion after continental breakup.

## CRediT authorship contribution statement

**Maxim Portnyagin:** Writing – review & editing, Writing – original draft, Visualization, Investigation, Formal analysis, Data curation, Conceptualization. **Antje Dürkefälden:** Writing – review & editing, Writing – original draft, Visualization, Investigation, Formal analysis, Data curation, Conceptualization. **Folkmar Hauff:** Writing – review & editing, Methodology, Data curation. **Andrey Gurenko:** Writing – review & editing, Methodology, Data curation. **Daniel A. Frick:** Writing – review & editing, Resources, Data curation. **Dieter Garbe-Schönberg:** Writing – review & editing, Resources, Methodology, Data curation. **Kaj Hoernle:** Writing – review & editing, Resources, Project administration, Funding acquisition, Conceptualization.

## Declaration of competing interest

The authors declare that they have no known competing financial interests or personal relationships that could have appeared to influence the work reported in this paper.

## Data availability

The authors declare that all data that support the findings of this study are available within the paper and its supplementary data (Tables S1-S5).

## Acknowledgments

The authors would like to thank Captain Mallon and the entire crew of the R/V SONNE cruise SO199 for their excellent support on board and S. Hauff, M. Thöner and U. Westernströer for analytical support. We also thank the German Ministry of Education and Research (BMBF) for financial support of the cruise and this study (03G0274A to K. Hoernle, F. Hauff and R. Werner) and GEOMAR Helmholtz Centre for Ocean Research Kiel for funding the analytical work. This research used samples from ODP Leg 123 provided by the Integrated Ocean Drilling Program. Marco Ligi and two anonymous reviewers are sincerely thanked for providing very helpful comments on early versions of this manuscript, and Rosemary Hickey-Vargas is thanked for editorial handling. We dedicate this paper to our late colleague Reinhard Werner.

## Supplementary materials

Supplementary material associated with this article can be found, in the online version, at doi:10.1016/j.epsl.2024.119021.

## References

Altherr, R., Henjes-Kunst, F., Puchelt, H., Baumann, A., 1988. Volcanic activity in the Red Sea axial trough — evidence for a large mantle diapir? Tectonophysics 150, 121–133. https://doi.org/10.1016/0040-1951(88)90298-3.

Anderson, D.L., 2005. Large igneous provinces, delamination, and fertile mantle. Elements 1, 271–275. https://doi.org/10.2113/gselements.1.5.271.

Ariskin, A.A., Barmina, G.S., 2004. COMAGMAT: development of a magma crystallization model and its petrological applications. Geochem. Int. 42 (1), S1–S157.

Armitage, J.J., Collier, J.S., Minshull, T.A., 2010. The importance of rift history for volcanic margin formation. Nature 465 (7300), 913–917. https://doi.org/10.1038/nature09063.

Bian, W., Yang, T., Ma, Y., Jin, J., Gao, F., Wang, S., Peng, W., Zhang, S., Wu, H., Li, H., Cao, L., Shi, Y., 2019. Paleomagnetic and geochronological results from the Zhela and Weimei formations lava flows of the eastern Tethyan Himalaya: new insights into the breakup of Eastern Gondwana. J. Geophys. Res.: Solid Earth 124, 44–64. https://doi.org/10.1029/2018JB016403.

Brandl, P.A., Regelous, M., Beier, C., Haase, K.M., 2013. High mantle temperatures following rifting caused by continental insulation. Nat. Geosci. 6, 391. https://doi.org/10.1038/ngeo1758.

Chen, S., Fan, W., Shi, R., Xu, J., Liu, Y., 2021. The Tethyan Himalaya Igneous Province: early melting products of the Kerguelen Mantle Plume. J. Petrol. 62. https://doi.org/10.1093/petrology/egab069.

Coltice, N., Phillips, B.R., Bertrand, H., Ricard, Y., Rey, P., 2007. Global warming of the mantle at the origin of flood basalts over supercontinents. Geology 35, 391–394. https://doi.org/10.1130/2FG23240A.1.

Connelly, J.N., Ulfbeck, D.G., Thrane, K., Bizzarro, M., Housh, T., 2006. A method for purifying Lu and Hf for analyses by MC-ICP-MS using TODGA resin. Chem. Geol. 233, 126–136. https://doi.org/10.1016/j.chemgeo.2006.02.020.

Courtillot, V., Jaupart, C., Manighetti, I., Tapponnier, P., Besse, J., 1999. On causal links between flood basalts and continental breakup. Earth Planet. Sci. Lett. 166, 177–195.

Crawford, A.J., von Rad, U., 1994. The petrology, geochemistry and implications of basalts dredged from the Rowley Terrace-Scott Plateau and Exmouth Plateau margins, northwestern Australia. J. Aust. Geol. Geophys. 15, 43–54.

Dixon, J.E., Bindeman, I.N., Kingsley, R.H., Simons, K.K., Le Roux, P.J., Hajewski, T.R., Swart, P., Langmuir, C.H., Ryan, J.G., Walowski, K.J., Wada, I., Wallace, P.J., 2017. Light stable isotopic compositions of enriched mantle sources: resolving the dehydration paradox. Geochem., Geophys., Geosyst. 18, 3801–3839. https://doi.org/10.1002/2016GC006743.

Dixon, J.E., Leist, L., Langmuir, C., Schilling, J.-G., 2002. Recycled dehydrated lithosphere observed in plume-influenced mid-ocean-ridge basalt. Nature 420, 385–389. https://doi.org/10.1038/nature01215.

Dürkefälden, A., Hauff, F., Hoernle, K., Portnyagin, M., Wartho, J.-A., Garbe-Schönberg, D., Gurenko, A., van den Bogaard, P., Kipf, A., Gutjahr, M., 2024. Geochemical and temporal evolution of Indian MORB mantle revealed by the Investigator Ridge in the NE Indian Ocean. Gondwana Res. 134, 347–364. https://doi.org/10.1016/j.gr.2024.07.016.

Fleck, R.J., Calvert, A.T., Coble, M.A., Wooden, J.L., Hodges, K., Hayden, L.A., van Soest, M.C., du Bray, E.A., John, D.A., 2019. Characterization of the rhyolite of Bodie Hills and 40Ar/39Ar intercalibration with Ar mineral standards. Chem. Geol. 525, 282–302. https://doi.org/10.1016/j.chemgeo.2019.07.022.

Franke, D., 2013. Rifting, lithosphere breakup and volcanism: comparison of magma-poor and volcanic rifted margins. Mar. Petrol. Geol. 43, 63–87. https://doi.org/10.1016/j.marpetgeo.2012.11.003.

Frey, F.A., Dickey Jr., J.S., Thompson, G., Bryan, W.B., 1977. Eastern Indian ocean DSDP sites: correlations between petrography, geochemistry and tectonic setting. In: Heirtzler, J.R., Bolli, H.M., Davies, T.A., Saunders, J.B., Sclater, J.G. (Eds.), Indian Ocean Geology and Biostratigraphy 9. American Geophysical Union, Washington, D. C., pp. 189–257

Fricker, M.B., Kutscher, D., Aeschlimann, B., Frommer, J., Dietiker, R., Bettmer, J., Günther, D., 2011. High spatial resolution trace element analysis by LA-ICP-MS using a novel ablation cell for multiple or large samples. Int. J. Mass Spectrom. 307, 39–45. https://doi.org/10.1016/j.ijms.2011.01.008.

Gale, A., Dalton, C.A., Langmuir, C.H., Su, Y., Schilling, J.-G., 2013. The mean composition of ocean ridge basalts. Geochem., Geophys., Geosyst. 14, 489–518. https://doi.org/10.1029/2012gc004334.

Gibbons, A.D., Barckhausen, U., van den Bogaard, P., Hoernle, K., Werner, R., Whittaker, J.M., Müller, R.D., 2012. Constraining the Jurassic extent of Greater India: Tectonic evolution of the West Australian margin. Geochem., Geophys., Geosyst. 13, Q05W13. https://doi.org/10.1029/2011GC003919.

Golowin, R., Portnyagin, M., Hoernle, K., Hauff, F., Gurenko, A., Garbe-Schönberg, D., Werner, R., Turner, S., 2017. Boninite-like intraplate magmas from Manihiki Plateau require ultra-depleted and enriched source components. Nat. Commun. 8, 14322. https://doi.org/10.1038/ncomms14322.

Golowin, R., Portnyagin, M., Hoernle, K., Hauff, F., Werner, R., Garbe-Schönberg, D., 2018. Geochemistry of deep Manihiki Plateau crust: implications for compositional diversity of large igneous provinces in the Western Pacific and their genetic link. Chem. Geol. 493, 553–566. https://doi.org/10.1016/j.chemgeo.2018.07.016.

Grigné, C., Labrosse, S., 2001. Effects of continents on Earth cooling: Thermal blanketing and depletion in radioactive elements. Geophys. Res. Lett. 28, 2707–2710.

Griffin, W., Powell, W., Pearson, N., O'Reilly, S., 2008. GLITTER: data reduction software for laser ablation ICP-MS. In: Laser Ablation-ICP-MS in the Earth Sciences, 40. Mineralogical association of Canada short course series, pp. 204–207.

Haase, K.M., Mühe, R., Stoffers, P., 2000. Magmatism during extension of the lithosphere: geochemical constraints from lavas of the Shaban Deep, northern Red Sea. Chem. Geol. 166, 225–239.

Herzberg, C., Asimow, P.D., 2008. Petrology of some oceanic island basalts: PRIMELT2. XLS software for primary magma calculation. Geochem. Geophys. Geosystems. 9, Q09001. https://doi.org/10.1029/2008gc002057.

Herzberg, C., Asimow, P.D., 2015. PRIMELT3 MEGA.XLSM software for primary magma calculation: peridotite primary magma MgO contents from the liquidus to the solidus. Geochem., Geophys., Geosyst. 16, 563–578. https://doi.org/10.1002/2014GC005631.

Herzberg, C., Asimow, P.D., Arndt, N., Niu, Y., Lesher, C.M., Fitton, J.G., Cheadle, M.J., Saunders, A.D., 2007. Temperatures in ambient mantle and plumes: Constraints from basalts, picrites, and komatiites. Geochem. Geophys. Geosystems. 8, Q02006. https://doi.org/10.1029/2006GC001390.

Hill, R.I., Campbell, I.H., Davies, G.F., Griffiths, R.W., 1992. Mantle plumes and continental tectonics. Science 256, 186–193. https://doi.org/10.1126/science.256.5054.186.

Hoernle, K., Abt, D.L., Fischer, K.M., Nichols, H., Hauff, F., Abers, G.A., van den Bogaard, P., Heydolph, K., Alvarado, G., Protti, M., Strauch, W., 2008. Arc-parallel flow in the mantle wedge beneath Costa Rica and Nicaragua. Nature 451, 1094–1097. https://doi.org/10.1038/nature06550.

Hoernle, K., Hauff, F., Kokfelt, T.F., Haase, K., Garbe-Schönberg, D., Werner, R., 2011a. On- and off-axis chemical heterogeneities along the South Atlantic Mid-Ocean-Ridge (5–11°S): Shallow or deep recycling of ocean crust and/or intraplate volcanism? Earth Planet. Sci. Lett. 306, 86–97. https://doi.org/10.1016/j.epsl.2011.03.032.

Hoernle, K., Hauff, F., Werner, R., van den Bogaard, P., Gibbons, A.D., Conrad, S., Muller, R.D., 2011b. Origin of Indian Ocean Seamount Province by shallow recycling of continental lithosphere. Nat. Geosci. 4, 883–887. https://doi.org/10.1038/ngeo1331.

Ishiwatari, A., 1992. Petrology, geochemistry, and mineralogy of the early cretaceous evolved N-MORB from sites 765 and 766, Eastern Indian Ocean In: Gradstein, F.M., Ludden, J.N., et al. (Ed.), Proceedings of the ODP Science Research, College Station, TX (Ocean Drilling Program), Vol. 123, pp. 201–213.

Jarosewich, E., Nelen, J.A., Norberg, J.A., 1980. Reference samples for electron microprobe analysis. Geostand. Newsl. 4, 43–47. https://doi.org/10.1111/j.1751-908X.1980.tb00273.x.

Jenner, F.E., O'Neill, H.S.C., 2012. Analysis of 60 elements in 616 ocean floor basaltic glasses. Geochem., Geophys., Geosyst. 13. https://doi.org/10.1029/2011GC004009.

Jochum, K.P., Verma, S.P., 1996. Extreme enrichment of Sb, Tl and other trace elements in altered MORB. Chem. Geol. 130, 289–299. https://doi.org/10.1016/0009-2541(96)00014-9.

Jochum, K.P., Stoll, B., Herwig, K., Willbold, M., Hofmann, A.W., Amini, M., Aarburg, S., Abouchami, W., Hellebrand, E., Mocek, B., Raczek, I., Stracke, A., Alard, O., Bouman, C., Becker, S., Dücking, M., Brätz, H., Klemd, R., de Bruin, D., Canil, D., Cornell, D., de Hoog, C.-J., Dalpé, C., Danyushevsky, L., Eisenhauer, A., Gao, Y., Snow, J.E., Groschopf, N., Günther, D., Latkoczy, C., Guillong, M., Hauri, E.H., Höfer, H.E., Lahaye, Y., Horz, K., Jacob, D.E., Kasemann, S.A., Kent, A.J.R., Ludwig, T., Zack, T., Mason, P.R.D., Meixner, A., Rosner, M., Misawa, K., Nash, B.P., Pfänder, J., Premo, W.R., Sun, W.D., Tiepolo, M., Vannucci, R., Vennemann, T., Wayne, D., Woodhead, J.D., 2006. MPI-DING reference glasses for in situ microanalysis: new reference values for element concentrations and isotope ratios. Geochem., Geophys., Geosyst. 7. https://doi.org/10.1029/2005GC001060.

Jochum, K.P., Weis, U., Stoll, B., Kuzmin, D., Yang, Q., Raczek, I., Jacob, D.E., Stracke, A., Birbaum, K., Frick, D.A., Günther, D., Enzweiler, J., 2011. Determination of reference values for NIST SRM 610–617 glasses following ISO guidelines. Geostand. Geoanal. Res. 35, 397–429. https://doi.org/10.1111/j.1751-908X.2011.00120.x.

Kelley, K., Plank, T., Grove, T.L., Stolper, E.M., Newman, S., Hauri, E., 2006. Mantle melting as a function of water content beneath back-arc basins. J. Geophys. Res. 111, B09208. https://doi.org/10.1029/2005JB003732.

Kimura, J.-I., Kawabata, H., 2015. Ocean Basalt Simulator version 1 (OBS1): trace element mass balance in adiabatic melting of a pyroxenite-bearing peridotite. Geochem., Geophys., Geosyst. 16, 267–300. https://doi.org/10.1002/2014gc005606.

King, S.D., Anderson, D.L., 1998. Edge-driven convection. Earth Planet. Sci. Lett. 160, 289–296. https://doi.org/10.1016/S0012-821X(98)00089-2.

Kogiso, T., Hirschmann, M.M., 2006. Partial melting experiments of bimineralic eclogite and the role of recycled mafic oceanic crust in the genesis of ocean island basalts. Earth Planet. Sci. Lett. 249, 188–199. https://doi.org/10.1016/j.epsl.2006.07.016.

Korenaga, J., 2004. Mantle mixing and continental breakup magmatism. Earth Planet. Sci. Lett. 218, 463–473. https://doi.org/10.1016/S0012-821X(03)00674-5.

Langmuir, C.H., Klein, E.M., Plank, T., 1992. Petrological systematics of mid-ocean ridge basalts: constraints on melt generation beneath ocean ridges, In: Morgan, J.P., Blackman, D.K., Sinton, J.M. (Eds.), Mantle Flow and Melt Generation at Mid-Oceanic Ridges, Vol. 71. American Geophysical Union, pp. 183–280.

Le Roux, V., Lee, C.T.A., Turner, S.J., 2010. Zn/Fe systematics in mafic and ultramafic systems: implications for detecting major element heterogeneities in the Earth's mantle. Geochim. Cosmochim. Acta 74 (9), 2779–2796. https://doi.org/10.1016/j.gca.2010.02.004.

Ligi, M., Bonatti, E., Tontini, F.C., Cipriani, A., Cocchi, L., Schettino, A., Bortoluzzi, G., Ferrante, V., Khalil, S., Mitchell, N.C., Rasul, N., 2011. Initial burst of oceanic crust accretion in the Red Sea due to edge-driven mantle convection. Geology 39 (11), 1019–1022. https://doi.org/10.1130/g32243.1.

Ligi, M., Bonatti, E., Bortoluzzi, G., Cipriani, A., Cocchi, L., Caratori Tontini, F., Carminati, E., Ottolini, L., Schettino, A., 2012. Birth of an ocean in the Red Sea: Initial pangs. Geochem., Geophys., Geosyst. 13 (8), Q08009. https://doi.org/10.1029/2012GC004155.

Ludden, J., et al., 1992a. Radiometric age determinations for basement from sites 765 and 766, Argo abyssal plain and Northwestern Australian Margin. In: Proceedings of the ODP Scientific Research, 123. Ocean Drilling Program, College Station, TX, pp. 557–559.

Ludden, J., Dionne, B., et al., 1992b. The geochemistry of oceanic crust at the onset of rifting in the Indian Ocean. In: Proceedings of the ODP Scientific Research, 123. Ocean Drilling Program, College Station, TX, pp. 791–799.

Magee, C., Jackson, C.A.L., 2020. Seismic reflection data reveal the 3D structure of the newly discovered Exmouth Dyke Swarm, offshore NW Australia. Solid Earth 11, 579–606. https://doi.org/10.5194/se-11-579-2020.

Melson, W.G., O'Hearn, T., Jarosewich, E., 2002. A data brief on the Smithsonian Abyssal Volcanic Glass Data File. Geochem., Geophys., Geosyst. 3, 1–11. https://doi.org/10.1029/2001GC000249.

Müller, R.D., Zahirovic, S., Williams, S.E., Cannon, J., Seton, M., Bower, D.J., Tetley, M. G., Heine, C., Le Breton, E., Liu, S., Russell, S.H.J., Yang, T., Leonard, J., Gurnis, M., 2019. A global plate model including lithospheric deformation along major rifts and Orogens Since the Triassic. Tectonics 38, 1884–1907. https://doi.org/10.1029/2018tc005462.

Ogg, J.G., 2020. Chapter 5 - geomagnetic polarity time scale. In: Gradstein, F.M., Ogg, J. G., Schmitz, M.D., Ogg, G.M. (Eds.), Geologic Time Scale 2020. Elsevier, pp. 159–192.

Pearce, J.A., 2005. Mantle preconditioning by melt extraction during flow: theory and petrogenetic implications. J. Petrol. 46, 973–997. https://doi.org/10.1093/petrology/egi007.

Portnyagin, M.V., Ponomareva, V.V., Zelenin, E.A., Bazanova, L.I., Pevzner, M.M., Plechova, A.A., Rogozin, A.N., Garbe-Schönberg, D., 2020. TephraKam: geochemical database of glass compositions in tephra and welded tuffs from the Kamchatka volcanic arc (northwestern Pacific). Earth Syst. Sci. Data 12, 469–486. https://doi.org/10.5194/essd-12-469-2020.

Roberge, J., White, R.V., Wallace, P.J., 2004. Volatiles in Submarine Basaltic Glasses from the Ontong Java Plateau (ODP Leg 192): Implications for Magmatic Processes and Source Region compositions. Geological Society, 229. Special Publications, London, pp. 239–257.

Rohrman, M., 2013. Intrusive large igneous provinces below sedimentary basins: an example from the Exmouth Plateau (NW Australia). J. Geophys. Res.: Solid Earth 118, 4477–4487. https://doi.org/10.1002/jgrb.50298.

Rohrman, M., 2015. Delineating the Exmouth mantle plume (NW Australia) from denudation and magmatic addition estimates. Lithosphere 7, 589–600. https://doi.org/10.1130/l445.1.

Seton, M., Müller, R.D., Zahirovic, S., Gaina, C., Torsvik, T., Shephard, G., Talsma, A., Gurnis, M., Turner, M., Maus, S., Chandler, M., 2012. Global continental and ocean basin reconstructions since 200 Ma. Earth-Sci. Rev. 113, 212–270.

Sobolev, S.V., Sobolev, A.V., Kuzmin, D.V., Krivolutskaya, N.A., Petrunin, A.G., Arndt, N. T., Radko, V.A., Vasiliev, Y.R., 2011. Linking mantle plumes, large igneous provinces and environmental catastrophes. Nature 477, 312–316. https://doi.org/10.1038/nature10385.

Sobolev, A.V., Asafov, E.V., Gurenko, A.A., Arndt, N.T., Batanova, V.G., Portnyagin, M. V., Garbe-Schönberg, D., Krasheninnikov, S.P., 2016. Komatiites reveal a hydrous

Archaean deep-mantle reservoir. Nature 531, 628–632. https://doi.org/10.1038/nature17152.

Steiger, R.H., Jäger, E., 1977. Subcommission on geochronology: Convention on the use of decay constants in geo- and cosmochronology. Earth Planet. Sci. Lett. 36, 359–362. https://doi.org/10.1016/0012-821X(77)90060-7.

Storey, B.C., Vaughan, A.P.M., Riley, T.R., 2013. The links between large igneous provinces, continental break-up and environmental change: evidence reviewed from Antarctica. Earth Environ. Sci. Trans. R. Soc. Edinburgh 104, 17–30. https://doi.org/10.1017/S175569101300011X.

Stracke, A., Bizimis, M., Salters, V.J.M., 2003. Recycling oceanic crust: quantitative constraints. Geochem., Geophys., Geosyst. 4. https://doi.org/10.1029/2001GC000223.

Sun, S.-S., McDonough, W.F., 1989. Chemical and isotopic systematics of oceanic basalts: implications for mantle composition and processes. In: Geological Society, 42. Special Publications, London, pp. 313–345. https://doi.org/10.1144/gsl.sp.1989.042.01.19.

van der Zwan, F.M., Devey, C.W., Augustin, N., Almeev, R.R., Bantan, R.A., Basaham, A., 2015. Hydrothermal activity at the ultraslow- to slow-spreading Red Sea Rift traced by chlorine in basalt. Chem. Geol. 405, 63–81. https://doi.org/10.1016/j.chemgeo.2015.04.001.

Wang, W., Chen, L., Dong, Y., Kelley, K.A., Chu, F., Zhou, B., Gong, B., Zhang, J., 2022. Development of major element proxies for magmatic H2O content in oceanic basalts. Chem. Geol. 610, 121068. https://doi.org/10.1016/j.chemgeo.2022.121068.

Wang, W., Kelley, K.A., Li, Z., Chu, F., Dong, Y., Chen, L., Dong, Y., Li, J., 2021. Volatile element evidence of local MORB mantle heterogeneity beneath the Southwest Indian Ridge, 48°–51°E. Geochem., Geophys., Geosyst. 22, e2021GC009647. https://doi.org/10.1029/2021GC009647.

Wang, Y., Zeng, L., Asimow, P.D., Gao, L., Ma, C., Antoshechkina, P.M., Guo, C., Hou, K., Tang, S., 2018. Early Cretaceous high-Ti and low-Ti mafic magmatism in Southeastern Tibet: Insights into magmatic evolution of the Comei Large Igneous Province. Lithos 296-299, 396–411. https://doi.org/10.1016/j.lithos.2017.11.014.

Weis, D., Frey, F.A., 1996. Role of the Kerguelen Plume in generating the eastern Indian Ocean seafloor. J. Geophys. Res.: Solid Earth 101, 13831–13849. https://doi.org/10.1029/96JB00410.

Werner, R., Hauff, F., Hoernle, K., 2009. RV SONNE Fahrtbericht /Cruise Report SO199 CHRISP, p. 85. https://doi.org/10.3289/ifmgeomar_rep_25_2009.

Willbold, M., Stracke, A., 2006. Trace element composition of mantle end-members: implications for recycling of oceanic and upper and lower continental crust. Geochem. Geophys. Geosyst. 7, Q04004. https://doi.org/10.1029/2005gc001005. Artn.

White, R., McKenzie, D., 1989. Magmatism at rift zones: the generation of volcanic continental margins and flood basalts. J. Geophys. Res.: Solid Earth 94, 7685–7729. https://doi.org/10.1029/JB094iB06p07685.

Workman, R.K., Hart, S.R., 2005. Major and trace element composition of the depleted MORB mantle (DMM). Earth Planet. Sci. Lett. 231, 53–72. https://doi.org/10.1016/j.epsl.2004.12.005.

Xia, Y., Zhu, D.-C., Wang, Q., Zhao, Z.-D., Liu, D., Wang, L.-Q., Mo, X.-X., 2014. Picritic porphyrites and associated basalts from the remnant Comei Large Igneous Province in SE Tibet: records of mantle-plume activity. Terra Nova 26, 487–494. https://doi.org/10.1111/ter.12124.

Zhu, D., Chung, S., Mo, X., Zhao, Z., Niu, Y., Song, B., Yang, Y., 2009. The 132 Ma Comei-Bunbury large igneous province: remnants identified in present-day southeastern Tibet and southwestern Australia. Geology 37, 583–586. https://doi.org/10.1130/g30001a.1.